# Influence of Hydroxyls on Pd Atom Mobility and Clustering on Rutile TiO$_2$(011)-2 × 1

Rafik Addou,[†,⊥] Thomas P. Senftle,[‡,⊥] Nolan O'Connor,[‡] Michael J. Janik,[‡,*] Adri C.T. van Duin,[§] and Matthias Batzill[†,*]

[†]Department of Physics, University of South Florida, Tampa, Florida 33620, United States and [‡]Department of Chemical Engineering, and [§]Department of Mechanical and Nuclear Engineering, Penn State University, University Park, Pennsylvania 16802, United States. [⊥]These authors contributed equally.

ABSTRACT Understanding agglomeration of late transition metal atoms, such as Pd, on metal oxide supports, such as TiO$_2$, is critical for designing heterogeneous catalysts as well as for controlling metal/oxide interfaces in general. One approach for reducing particle sintering is to modify the metal oxide surface with hydroxyls that decrease adatom mobility. We study by scanning tunneling microscopy experiments, density functional theory (DFT) calculations, and Monte Carlo (MC) computer simulations the atomistic processes of Pd sintering on a hydroxyl-modified TiO$_2$(011)-2 × 1

surface. The formation of small 1—3 atom clusters that are stable at room temperature is achieved on the hydroxylated surface, while much larger clusters are formed under the same conditions on a hydroxyl-free surface. DFT shows that this is a consequence of stronger binding of Pd atoms adjacent to hydroxyls and increased surface diffusion barriers for Pd atoms on the hydroxylated surface. DFT, kinetic MC, and ReaxFF-based NVT-MC simulations show that Pd clusters larger than single Pd monomers can adsorb the hydrogen from the oxide surface and form Pd hydrides. This depletes the surface hydroxyl coverage, thus allowing Pd to more freely diffuse and agglomerate at room temperature. Experimentally, this causes a bimodal cluster size distribution with 1—3 atom clusters prevalent at low Pd coverage, while significantly larger clusters become dominant at higher Pd concentrations. This study demonstrates that hydroxylated oxide surfaces can significantly reduce Pd cluster sizes, thus enabling the preparation of surfaces populated with metal clusters composed of single to few atoms.
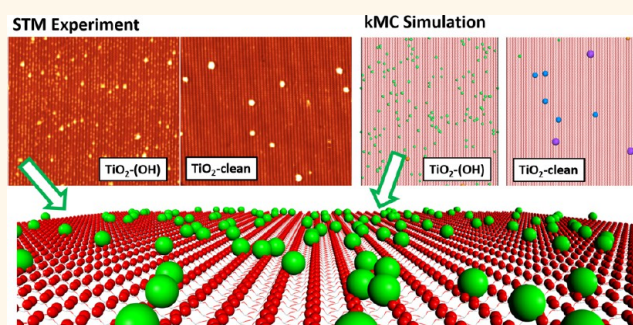
KEYWORDS: palladium · metal clusters · titania · oxide surfaces · scanning tunneling microscopy · density functional theory · ReaxFF

Diffusion and agglomeration of metal adatoms on oxide surfaces plays an important role in the creation of nanoparticles and, more generally, in the formation of metal/oxide interfaces. The dispersion of transition metals and their agglomeration into clusters on metal oxide supports is of particular interest for the formation of catalytically active metal nanoclusters. Single-atom catalysts,[1−3] as well as cluster-size-dependent chemical functionality, have been documented.[4] Notably for gold, numerous studies demonstrate a dramatic effect of cluster size on catalytic activity.[5−11] Similarly, Pd clusters display numerous size-dependent chemical properties.[12−17] In addition to catalysis, the agglomeration of metal atoms into clusters also affects the formation of ultrathin metal coatings on metal oxides. In order to synthesize and maintain small clusters, adatom mobility and sintering must be suppressed. For planar model catalysts used in fundamental surface science studies, transition metals are commonly vapor-deposited on oxide supports. However, vapor deposition of transition metals at room temperature on oxide supports usually results in nanometer-sized clusters with several hundred atoms, which precludes investigation of very small nanoclusters. In addition, to address the technologically important issue of oxide wetting with metal layers, hydroxylation of oxides has been suggested as a means for increasing metal binding.[18−20] Thus, the formation of very small metal clusters, as well as metal coatings, may be controlled by hydroxyls on oxide surfaces.
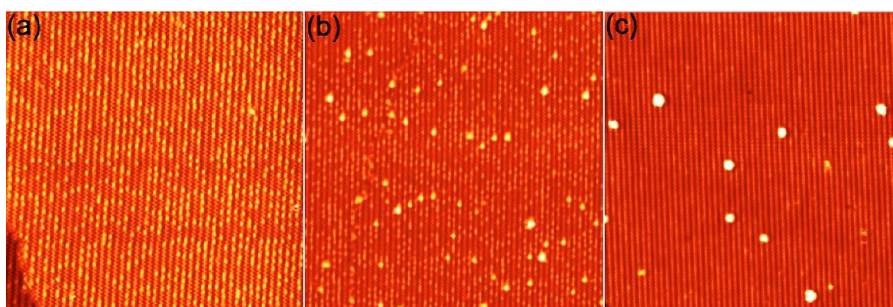
Figure 1. STM characterization of $TiO_2(011)$-2 × 1 surfaces. (a) Partially hydroxylated TiO_2 surface, with the bright spots indicating individual hydroxyl groups (40 nm × 40 nm, V_{bias} = 1.3 V, I_t = 0.4 nA). (b) Hydroxylated TiO_2 surface after deposition of small amount of Pd (50 nm × 50 nm, V_{bias} = 1.3 V, I_t = 0.5 nA). (c) Deposition of the same amount of Pd as in (b) on an almost hydroxyl-free surface (50 nm × 50 nm, V_{bias} = 1.3 V, I_t = 0.5 nA). The Pd cluster sizes are small, typically only 1−3 atoms, in (b) compared to much larger clusters in (c).

Unfortunately, the fundamental processes governing metal−hydroxyl interactions on oxide surfaces are not well-understood. Here we combine scanning tunneling microscopy with computer simulations to investigate the interplay between hydroxyls and transition metal atoms, thus yielding atomic level insight into the effect of oxide hydroxylation on metal cluster formation.

Numerous scanning tunneling microscopy (STM) studies of vapor-deposited metals on planar oxide model systems have contributed to the understanding of metal diffusion and agglomeration.[21−23] The majority of these studies focused on pristine metal oxide surfaces, while some investigated the role of impurities,[24] particularly hydroxyls, on metal cluster formation. Matthey et al. investigated the bonding of Au on $TiO_2(110)$ for variously prepared surfaces.[25] For hydroxylated surfaces, an apparent decreased adhesion of Au was found resulting in the formation of large Au clusters compared to vacuum-prepared $TiO_2(110)$ surfaces, which contain O vacancies. Conversely, hydroxyls on Fe_3O_4 surfaces induced stronger Pd binding and reduced sintering.[26] Previous DFT studies for Ag on hydroxylated alumina[27,28] also suggest that the interaction strength between the hydroxyl and the transition metal adatoms is important for determining the sintering behavior of transition metals.

Here we use STM experiments in conjunction with DFT calculations, kinetic Monte Carlo (kMC) simulations, and ReaxFF-based Monte Carlo simulations to investigate Pd adatom behavior on pristine and hydroxylated $TiO_2(011)$-2 × 1 surfaces. At low Pd coverage, the hydroxyl groups effectively suppress surface diffusion, leading to small Pd clusters that are stable at room temperature. This is contrasted by the formation of large Pd clusters on the pristine surface. Furthermore, simulations show that Pd clusters as small as two atoms can remove hydrogen from the $TiO_2(011)$-2 × 1 surface and adsorb it on the Pd clusters. This process is made possible by the known weak binding of hydrogen to the $TiO_2(011)$- 2 × 1 surface.[29] An obvious consequence of removing the hydroxyls from the TiO_2 surface is that this process causes the hydrogen-induced increase in the diffusion barrier for Pd adatoms to disappear. This then facilitates sintering of Pd to a level similar to that of an initially hydroxyl-free surface. Thus, at a Pd coverage that is high enough to remove all the hydroxyls from the TiO_2 surface, the sintering and agglomeration of Pd are expected to be undistinguishable or at least very similar to that on an initially hydroxyl-free surface. Generally, our atomistic studies demonstrate that hydroxyls on oxide surfaces can strongly affect the diffusion and sintering of metals. However, on this particular TiO_2 surface, two Pd atoms are sufficient to remove one hydroxyl from the TiO_2 surface and consequently remove the additional Pd diffusion barrier the hydroxyls introduce. Thus, only single Pd atoms, and possibly dimers and trimers, are prevented from sintering. A 2 atom Pd cluster can only adsorb one hydrogen, and thus additional hydroxyls at the surface can still prevent diffusion of Pd atoms from such a Pd_2H cluster. This explains the presence of 2 and 3 atom clusters in STM images on a hydroxylated surface at low coverage (Figure 1b). Importantly, the agreement between the experiment and simulation validates our theoretical description, providing rationale for screening methods that could identify metal oxide systems that may yield high concentrations of small clusters that are resistant to sintering at room temperature.

RESULTS

Scanning Tunneling Microscopy Investigation of Pd Cluster Formation. Pd atoms were vapor-deposited on the 2 × 1 reconstructed rutile $TiO_2(011)$ surface[30−33] held at room temperature. For low doses of Pd, the adsorption structure on a clean $TiO_2(011)$-2 × 1 surface is compared to that of a hydroxylated surface in Figure 1. In Figure 1a, a hydroxylated surface prior to Pd deposition is shown. The hydroxyls appear in the STM images as bright protrusions situated slightly off-center of the characteristic zigzag rows of the $TiO_2(011)$-2 × 1. The adsorption of the hydroxyls on this surface is discussed in more detail in ref 29. Figure 1b shows the surface
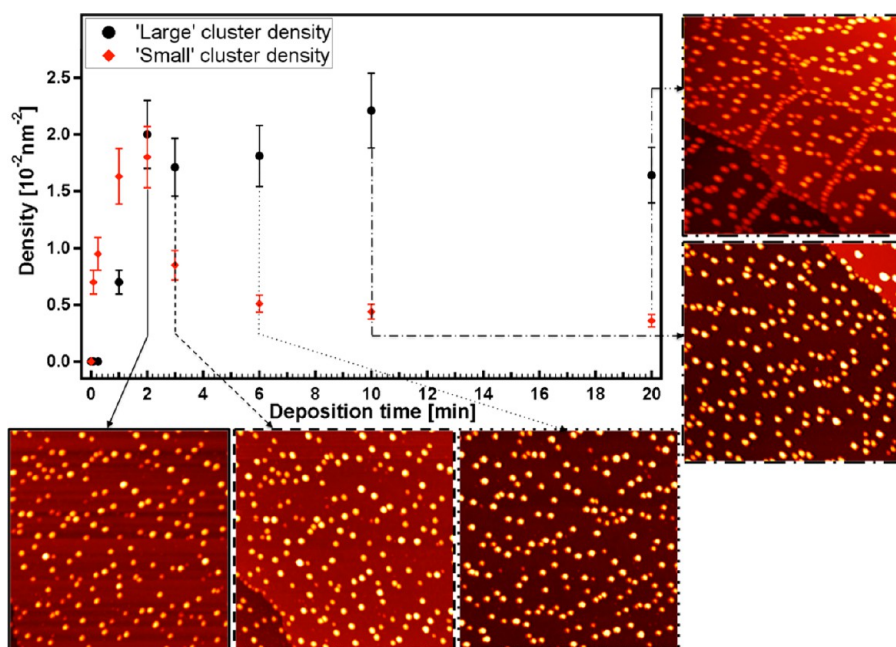
Figure 2. Evolution of cluster density as a function of deposition time on an initially hydroxylated TiO$_2$(011)-2 × 1 surface. We distinguish between small clusters with an estimated 1−3 Pd atoms and larger clusters, whose height suggests at least 2−3 atom layer height. The density of small clusters is shown as red diamonds and the cluster density for the larger clusters as black circles. Representative STM images of the surface structure for different Pd deposition times are shown. All STM images are 100 nm × 100 nm in size. For low deposition times, see Figure 1b.

after the deposition of a small amount of Pd on a surface exhibiting hydroxyls, while Figure 1c shows the same amount of Pd deposited on a nearly hydroxyl-free surface. Clearly, a higher density of clusters is observed in Figure 1b than in Figure 1c, and consequently, the clusters in (b) are smaller than in (c). All the Pd-associated features in Figure 1b have similar apparent heights (2.1−3 Å). Only three different lateral sizes are observed. These different sizes are assigned to clusters with one, two, or three Pd atoms. Particularly, the smallest clusters, which may be associated with single Pd atoms, are situated close to the zigzag row in STM. Also seen in Figure 1b, an antiphase domain boundary of the 2 × 1 reconstruction is visible running from the top to the bottom of the STM image. While we show below that such defects are preferential "anchor sites" for larger Pd clusters, for the low Pd density shown in Figure 1b, no statistically significant increased Pd cluster formation along such defects is observed.

On the hydroxyl-free surface, the cluster height and lateral dimensions are significantly larger. For an identical Pd amount as for the hydroxylated surface shown in Figure 1b, the cluster heights are mainly in the range of 3.6−6.5 Å, indicating that the clusters are much larger in size and have a 3D cluster shape that may be as much as three atoms tall. Furthermore, the smaller density of clusters, for nominally the same amount of Pd, also indicates the larger size of the clusters. The differences in size and density of Pd clusters for the hydroxyl-free surface compared to the partially

hydroxylated surface suggests that Pd atoms have very different mobility on these two surfaces. An obvious assessment is that, on the hydroxylated surface, Pd atoms cannot diffuse over long distances and consequently do not sinter into larger clusters.

Staying with an initially hydroxylated surface, we investigated the cluster evolution as a function of the amount of deposited Pd. A Pd evaporation source with constant Pd flux is used, so that the amount of Pd is proportional to the deposition time. Thus, we consider the deposition time a measure of the amount of Pd deposited. As noted above, for Pd deposition time of less than 1 min, we observe only clusters of ~1−3 atoms in size. For Pd deposition times of 1−3 min, we observe a bimodal cluster size distribution. In addition to the small clusters, clusters larger and taller are observed with a height of 3−6 Å. These larger clusters are comparable to the clusters observed at low Pd coverage on the hydroxyl-free surface.

Figure 2 shows the cluster densities for the "small" and "large" clusters as a function of Pd deposition time. For very low deposition times, only small clusters are present. With increasing Pd deposition time, initially, the density of both small and large clusters increases. After 2 min of deposition, the density of small clusters decreases while the density of large clusters remains nearly constant. This suggests that the small clusters have been incorporated into the larger clusters. With increasing Pd deposition, the clusters continue to grow, though no new large clusters are nucleated once a critical density has been reached. In addition,
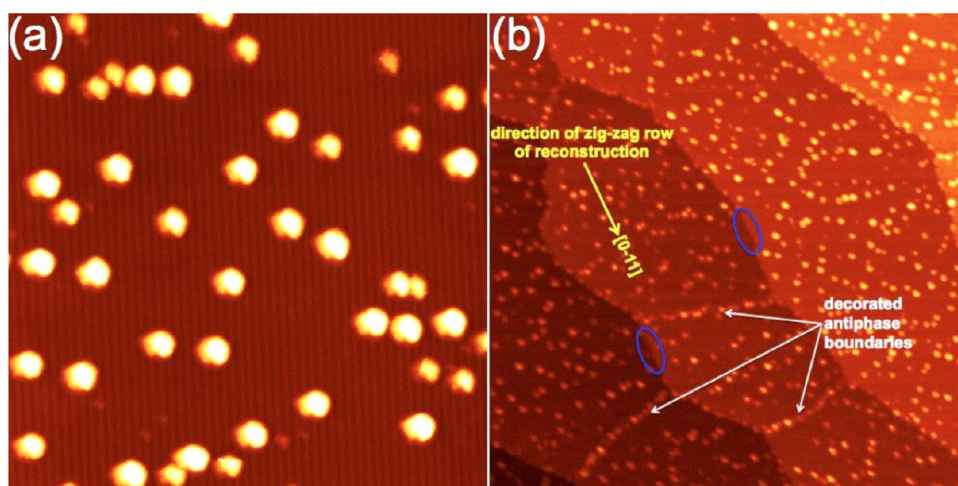
Figure 3. Pd clusters on a TiO$_2$(011)-2 × 1 after long (6 min) Pd deposition. The surface in (a) was hydroxyl-modified prior to Pd deposition (50 nm × 50 nm, V_{bias} = 1.3 V, I_t = 0.5 nA). No hydroxyls remain at the surface, suggesting that the Pd clusters have absorbed the surface hydrogen. The same asymmetry of all the clusters are due to a "tip artifact" that modifies the imaging of the taller clusters but does not affect the imaging of the hydroxyls, that is, the absence of hydroxyls. The STM image in (b) shows a 170 nm × 170 nm area (V_{bias} = 1.3 V, I_t = 0.4 nA). The decoration of antiphase domain boundaries of the 2 × 1 surface reconstruction by Pd clusters can be observed (white arrows). Also step edges are decorated with Pd; however, steps that are oriented parallel to the row structure of the surface reconstruction are not decorated (blue ovals), indicating preferential Pd diffusion in the direction of the Pd rows.

hydroxyls between the clusters disappear with increasing Pd deposition. At the point of maximum cluster density (*i.e.*, after ~3 min deposition time), almost no hydroxyls remain at the surface. The absence of hydroxyls can be seen in the higher resolution image shown for 6 min deposition time in Figure 3a. Furthermore, the decoration of step edges and antiphase domain boundaries with larger Pd clusters is seen in Figure 3b after 20 min of deposition time. Step edges that are parallel to the [0$\overline{1}$1] direction, that is, parallel to the row structure of the surface reconstruction, show less decoration than step edges that intersect the surface row structure. This indicates that Pd atoms preferentially diffuse along the rows and are anchored at step edges that intersect this diffusion direction. Preferential diffusion along the rows of the reconstruction is consistent with a lower diffusion barrier in this direction, in agreement with computed diffusion barriers discussed below. While a preferred diffusion direction is a kinetic effect, the decoration of step edges and antiphase boundaries may indicate that binding at these defects is also enhanced, as has been observed for metal clusters on many other oxide supports.[34−36]

These experimental results suggest the following mechanisms. At low Pd coverage, hydroxyls prevent diffusion of Pd atoms, resulting in small Pd clusters consisting of only 1−3 Pd atoms. Furthermore, the disappearance of hydroxyls from the oxide surface for Pd deposition times longer than ~3 min suggests that larger Pd clusters take up hydrogen, which subsequently makes Pd adatoms more mobile and facilitates the formation of larger clusters. This uptake of hydrogen by Pd clusters is confirmed below in
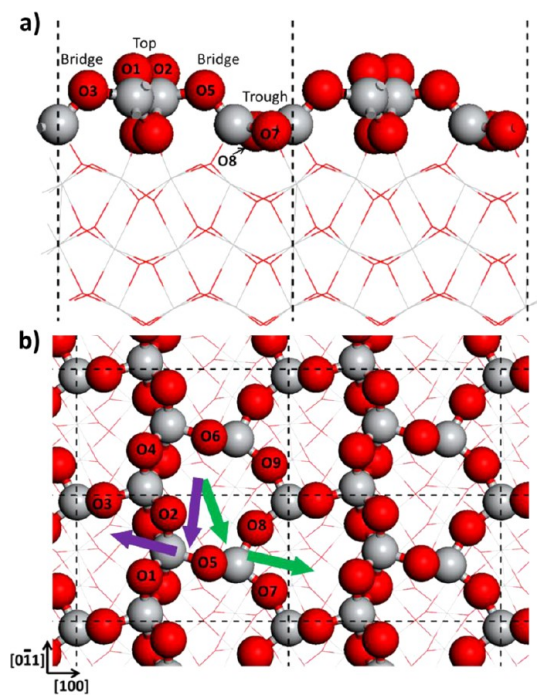
computer simulations. The alternative explanation that the deposition of Pd atoms causes thermal desorption of hydrogen from the TiO$_2$ surface is unlikely because of the previously reported thermal behavior of hydrogen on this surface.[29] To substantiate the influence of hydroxyls on Pd adsorption, we performed a series of computational analyses, which are discussed in the following sections.

Simulation of Pd Diffusion Barriers. Both DFT and classical computational techniques are employed to assess the various aspects of Pd diffusion, cluster formation, and hydrogen uptake on the clean and hydroxylated TiO$_2$(011)-2 × 1 surface. To determine the effect of adsorbed hydrogen on Pd mobility, DFT calculations are used to derive the potential energy surface for varying Pd diffusion paths over the clean and hydroxylated surfaces. The barriers and adsorption energies derived with DFT calculations are then employed in kinetic Monte Carlo simulations to assess cluster formation rates. Finally, a Ti/O/Pd/H ReaxFF potential is employed in Monte Carlo simulations to assess hydrogen transfer between the TiO$_2$ surface and Pd clusters of varying size.

DFT calculations were completed on two models of the TiO$_2$(011)-2 × 1 surface, consisting of a clean surface (shown in Figure 4) and a hydroxylated surface. The clean surface contains characteristic zigzag rows separated by a trough region containing alternating hollow sites. The unit cell contains two top oxygen atoms in the zigzag row (labeled O1 and O2, where O4 is the periodic image of O1), two trough oxygen atoms (labeled O7 and O8, where O9 is the periodic image of O7), and two bridging oxygen atoms located on opposite sides of the zigzag row (labeled O3 and O5,

where O6 is the periodic image of O5). The hydroxylated surface model is obtained by adsorbing a single H atom in the unit cell above top oxygen O1, which is the previously determined preferred hydrogen adsorption site.[29]
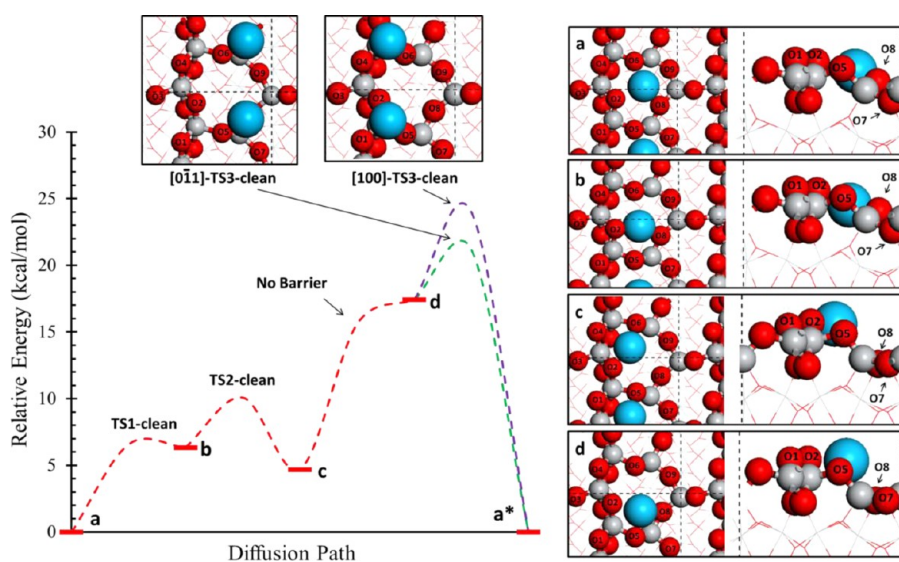
On the clean surface, a single Pd atom adsorbs most strongly in the hollow site of the trough between oxygen atoms O6 and O8, with an exothermic adsorption energy of -50.7 kcal mol^{-1} relative to the clean surface and a single gas-phase Pd atom. Similarly on the hydroxylated surface, the Pd atom binds most strongly in the hollow site between oxygen atoms O2 and O6, with an exothermic adsorption energy of -55.3 kcal mol^{-1}. Net diffusion in the [0$\bar{1}$1] direction parallel to the zigzag row consists of Pd migration between adjacent hollow sites within the same trough, and net diffusion in the [100] direction perpendicular to the zigzag row consists of Pd migration between adjacent hollow site separated by the row structure. The overall diffusion barrier for each direction can be assessed by determining the minimum energy path for Pd migration between adjacent sites in the trough (represented by green arrows in Figure 4) or between adjacent sites separated by the zigzag row structure (represented by purple arrows).

The minimum energy paths for Pd migration on the clean TiO$_2$ surface are shown in Figure 5. As seen in the figure, we identified energy minima within the hollow site between oxygen atoms O2–O8 (Figure 5b) and between oxygen atoms O2–O6 (Figure 5c) that are 6.3 and 4.7 kcal mol^{-1} higher in energy than the preferred hollow site (Figure 5a), respectively. Figure 5d depicts a metastable adsorption site between oxygen atoms O8–O5, from which the Pd atom may migrate into the adjacent hollow site within the trough by traversing the bridging oxygen O8, or may migrate over the row by traversing top oxygen atoms O1–O2. The overall activation barriers for these two processes are 21.2 and 24.0 kcal mol^{-1}, respectively, where the transition state structures identified for these two paths are depicted in the insets of the figure. Using a simple Arrhenius relationship, we approximate that

Figure 4. (a) Side and (b) top views of the TiO$_2$(011)-2 × 1 surface. Surface atoms are represented by spheres, and bulk atoms are represented by lines. The dashed lines indicate the unit cell used in all calculations. Purple arrows indicate the Pd diffusion path parallel to the [100] direction traversing the top oxygens of the zigzag row. The green arrows indicate the Pd diffusion path traversing trough oxygens between adjacent hollow sites parallel to the [0−11] direction.

Figure 5. Diffusion barrier over the clean TiO$_2$ surface for Pd migration between hollow sites traversing top oxygens (purple) and traversing trough oxygens (green). Energy-minimized structures are shown to the right, and transition state structures are shown in the insets above. Symmetrically equivalent positions in adjacent hollow sites are marked with a star.
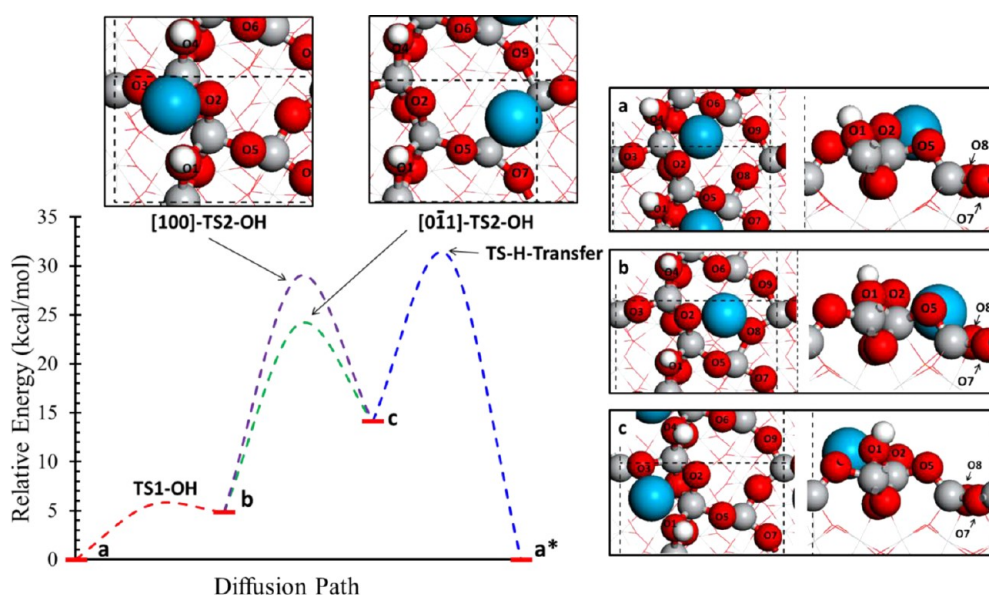
Figure 6. Diffusion barrier over the hydroxylated TiO₂-(OH) surface for Pd migration between hollow sites traversing top oxygens (purple) and traversing trough oxygens (green). The blue line represents the barrier for a hydrogen transfer from oxygen "O4" to oxygen "O2". Energy-minimized structures are shown to the right, and transition state structures are shown in the insets. Symmetrically equivalent sites are marked with a star.

diffusion in the [0$\bar{1}$1] direction parallel to the zigzag row is ~1.1 × 10² times faster than diffusion in the [100] direction at 300 K, in agreement with the experimental observations described above.

Figure 6 depicts the calculated minimum energy paths for Pd migration on the hydroxylated TiO₂ surface. In addition to the preferred adsorption site in the surface hollow between O2 and O6 (Figure 6a), we identified an energy-minimized site in the surface hollow between O2 and O8 (Figure 6b) that is 4.9 kcal mol⁻¹ higher in energy than the preferred site. Again, from this site, the Pd atom can migrate to an adjacent hollow site within the trough by traversing trough oxygen O8 or can diffuse into the adjacent trough by traversing top oxygen O2. The transition state structures for each of these paths are shown in the insets of the figure, yielding overall diffusion barriers of 24.1 and 28.9 kcal mol⁻¹ for diffusion in the [0$\bar{1}$1] direction and [100] direction, respectively. Similar to the clean surface, diffusion in the [0$\bar{1}$1] direction is preferred and occurs ~3.1 × 10³ times faster at 300 K than diffusion in the [100] direction perpendicular to the zigzag row. Compared to the clean surface, the diffusion barrier in the [0$\bar{1}$1] direction yields a diffusion rate ~1.3 × 10² times slower than the rate over the analogous path on the clean surface. Likewise, the barrier in the [100] direction yields a diffusion rate ~3.7 × 10³ times slower than the analogous rate on the clean surface. These results corroborate the above experimental observations by demonstrating that hydroxyl groups on the TiO₂ surface hinder Pd diffusion rates, thus preventing the agglomeration of Pd atoms into large clusters.

Unlike the clean surface, adjacent hollow sites on the hydroxylated surface are not necessarily equivalent, as the additional hydrogen atom can be adsorbed on either top oxygen O1 or O2, which breaks the symmetry of the unit cell. This is illustrated in the figure, where the most stable site in the adjacent hollow (Figure 6c) yields an adsorption energy 14.1 kcal mol⁻¹ higher than the preferred site. The equivalent of the optimal adsorption site can be obtained by transferring the adsorbed hydrogen from O1 to O2, which is depicted by the blue dashed line in the figure. The barrier for hydrogen transfer is 17.0 kcal mol⁻¹ relative to the structure shown in Figure 6c, which is similar to the barrier of 17.3 kcal mol⁻¹ reported for the analogous hydrogen transfer in the absence of adsorbed Pd.[29] The barrier for the reverse hydrogen transfer process is 31.2 kcal mol⁻¹, indicating that adsorbed Pd atoms hinder H diffusion across the TiO₂ surface. Ultimately, this does not affect the overall diffusion barrier for a complete Pd migration step, as the barrier for Pd migration from the adsorption site shown in Figure 6c to the next adjacent hollow site is simply the reverse of the *a-to-c* barrier shown in the figure, which is lower than the H transfer barrier shown in blue. Hence, the apparent diffusion barriers for Pd migration consist of the paths shown in green and purple in Figure 6.

Kinetic Monte Carlo Simulation of Pd Sintering. We employed kMC simulations to further assess the impact of hydroxyl groups on Pd cluster formation. These simulations utilize a simple sintering model,[37] in which Pd clusters are considered immobile and cluster growth occurs through the exchange of single Pd atoms between clusters. A similar kMC model was
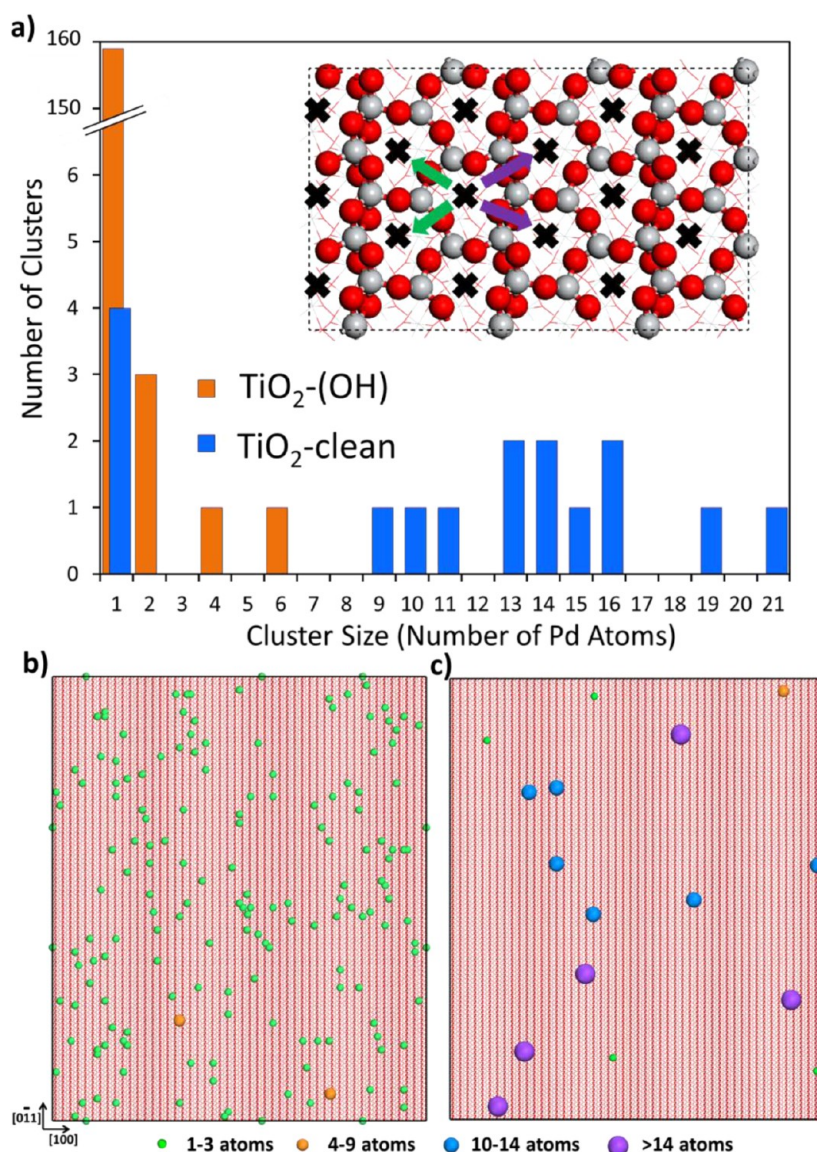
Figure 7. (a) Final cluster size distribution after kinetic Monte Carlo simulations of Pd sintering on the clean and hydroxylated TiO$_2$ surfaces for 3 s at 450 K. The inset depicts the grid employed during the simulation, where green arrows represent moves between adjacent hollow sites within the trough and purple arrows represent moves between hollow sites separated by a zigzag row. (b,c) Final cluster distribution projected onto the corresponding 55 nm × 46 nm (b) clean and (c) hydroxylated surfaces. Sphere size and color represents cluster size range: 1−3 atoms (small, green), 4−9 atoms (medium-small, orange), 10−14 atoms (medium-large, blue), and >14 atoms (large, purple).

applied by Zhang and Alexandrova[38] to model Pd cluster growth on defective TiO$_2$(110) surfaces, demonstrating the feasibility of this approach for modeling Pd mobility on titania. To represent the TiO$_2$(011)-(2 × 1) surface, we constructed a two-dimensional lattice, shown in the inset of Figure 7a, where every lattice position represents a Pd adsorption site in the preferred hollow position. During the simulation, single Pd atoms are exchanged between hollow sites, and the occupancy at each lattice position represents the cluster size at that adsorption site. The corresponding rate for each move is calculated from harmonic transition state theory, which is described in the Methods section along with further details of the kMC method.

To simulate the sintering behavior observed experimentally in Figure 1, we performed each kMC simulation with a 100 × 100 lattice populated with 175 Pd atoms placed in random lattice positions. This lattice size and Pd adsorption density yields a 55 nm × 46 nm surface with a 0.0175 ML coverage of Pd, which is comparable to the experimental STM images shown in Figure 1. Each kMC simulation was conducted at 450 K for 3 s, which was sufficient to induce sintering on the clean surface. The results, shown in Figure 7, demonstrate that the elevated barriers on the hydroxylated surface effectively prevent cluster growth, as the majority of Pd atoms remain as monomers. Conversely, Pd atoms aggregate into larger Pd clusters on the clean
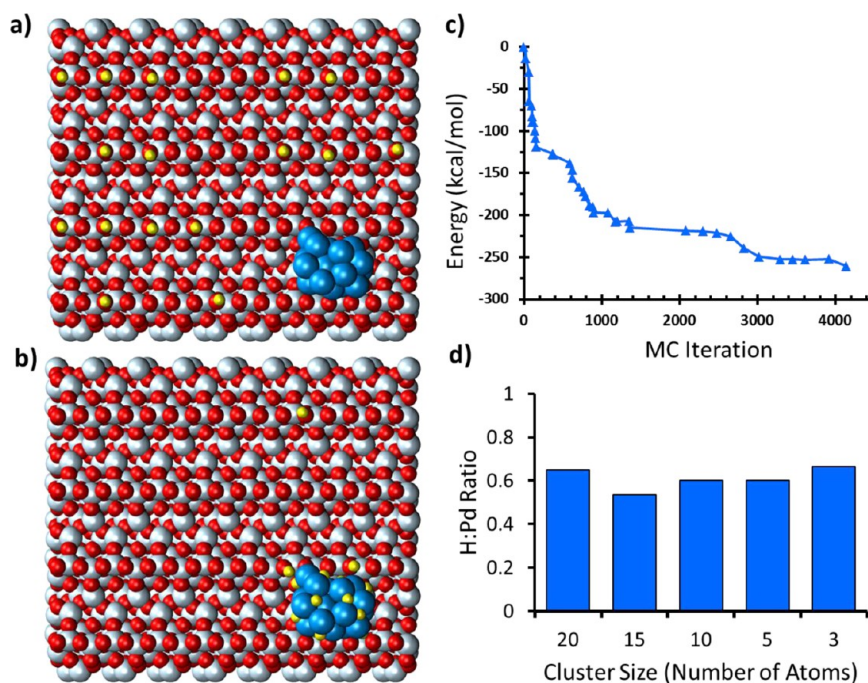
Figure 8. (a) Initial and (b) final structure of a NVT-MC simulation of PdH formation initiated from a clean Pd_{20} cluster adsorbed on the TiO_2 surface. (c) Convergence of the total system energy as hydrogen is adsorbed by the Pd cluster. (d) Final H/Pd ratios from converged simulations initiated with Pd_n cluster sizes ranging from $n = 20$ to $n = 3$.

surface, where only a few Pd atoms remain as monomers. The final cluster distributions, shown in Figure 7b, c, closely resemble the STM results shown in Figure 1, demonstrating the feasibility of the kMC sintering model. Nevertheless, these results are limited in that they assume that all adsorption sites are equivalent, and that the formation of clusters does not affect adsorption energies or barriers in adjacent sites. Furthermore, this model assumes that only Pd monomers are mobile, whereas it is possible that slightly larger Pd clusters (dimers and trimers) are also mobile. We assume that diffusion hindrance observed for Pd monomers will similarly apply to slightly larger clusters, and the qualitative conclusions are not affected. Despite these limitations, this simplified kMC model further illustrates the kinetic effect of surface hydroxyl groups on cluster formation identified in the DFT energetics in the previous section, demonstrating agreement with our experimental observations.

ReaxFF Simulation of Pd Hydride Formation. Clusters of Pd hydride may form on the TiO_2 surface, which was suggested in the experimental observation that the coverage of hydroxyl groups significantly decreased with the formation of larger Pd clusters. To investigate the thermodynamic preference for hydrogen to exchange between adsorption sites on the TiO_2 surface and the supported Pd clusters, we conducted MC simulations utilizing ReaxFF interaction parameters for Pd/Ti/O/H. These simulations featured MC steps where H atoms are randomly displaced in a unit cell consisting of a Pd cluster supported on a TiO_2 surface.

The initial system, shown in Figure 8a, consisted of a 4×8 supercell built from the 2×1 unit cells employed in the DFT calculations. The supercell contains 16 H atoms distributed randomly in the preferred atop sites, yielding a hydrogen coverage of 0.2 ML. Simulations were repeated with varying cluster sizes, where each Pd_n cluster model was structurally optimized by choosing the lowest energy structure after using stochastic MC steps to sample multiple random configurations of the isolated cluster at 300 K. The optimized cluster model was then adsorbed on the TiO_2 surface in a hollow site and was then further optimized using a conjugant gradient relaxation of forces.

Using the cluster/surface model, MC steps consisting of a random H atom displacement were executed until the total system energy converged. The probability of accepting the resulting geometry after a MC trial step was determined by the usual Metropolis criteria and is further described in the Methods section. The results, summarized in Figure 8, demonstrate that H atoms generally prefer adsorption sites on the Pd cluster. This is demonstrated in Figure 8b, where nearly all of the H atoms initially present on the TiO_2 surface have migrated to the Pd_{20} cluster. Similar results were obtained for smaller clusters, shown in Figure 8d, where the final H/Pd ratio in the cluster remains near ~0.6 in all cluster sizes, which is the ratio typically observed in the Pd hydride phase.[39−42] In simulations with smaller clusters, excess H atoms remained on the TiO_2 surface after the Pd cluster became saturated with hydrogen. Additional DFT calculations were completed
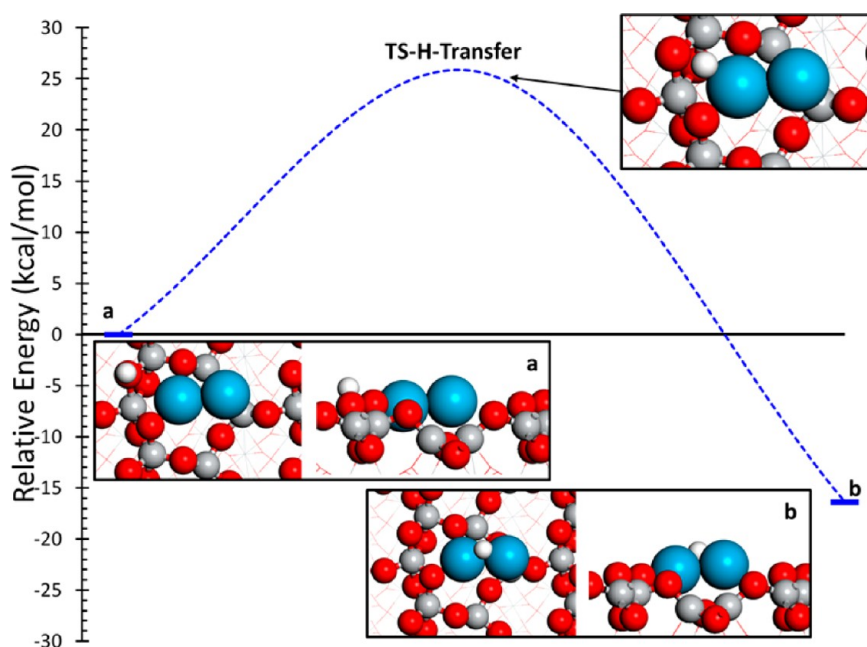
Figure 9. DFT minimum energy path for hydrogen transfer from a surface hydroxyl group to a Pd dimer. (Inset) Initial, final, and transition state structures.

to assess H uptake by Pd monomers and dimers. As shown in Figure 9, hydrogen adsorption on the Pd dimer is 16.3 kcal mol^{-1} more favorable than H adsorption on the oxide surface, and the migration barrier for a H atom to move from the oxide to the dimer is 25.6 kcal mol^{-1}. This indicates that it is thermodynamically favorable for the Pd dimer to adsorb a hydrogen from an adjacent hydroxyl, but that the kinetics of this process will be slow at room temperature. It is reasonable to assume that this barrier will be significantly lower for migration to larger clusters since larger clusters have a greater quantity of favorable adsorption sites leading to less constrained migration paths. H adsorption on the Pd monomer was 6.67 kcal mol^{-1} less favorable than adsorption on the oxide, indicating that it is thermodynamically unfavorable for a single Pd atom to remove a surface hydroxyl group.

These results corroborate the experimental findings reported above, in which H atoms from hydroxyl groups are absorbed by Pd clusters. The simulations suggest that there is a maximum H/Pd ratio in the clusters similar to that of the Pd hydride phase (~0.6), and that additional hydrogen will remain on the surface after this limit is reached in the Pd clusters. Hence, at low Pd deposition times, many hydroxyl groups remain on the surface, inhibiting the formation of large Pd clusters. After a critical Pd deposition time, enough Pd clusters are on the surface to remove all hydroxyl groups, thus reducing Pd diffusion barriers leading to the formation of larger clusters.

DISCUSSION

The effect of hydroxyl groups on the sintering behavior of Pd clusters adsorbed on a planar rutile

TiO$_2$(011)-2 × 1 surface has been investigated with combined experimental and computational techniques. TiO$_2$ is an important photocatalyst. However, in photocatalytic applications, typically a mixture of anatase and rutile polymorphs is used with the anatase polymorph being more photocatalytically active as a consequence of their bulk properties.[43] Pure rutile TiO$_2$, on the other hand, may be used as traditional oxide support in heterogeneous catalysts. In addition to these important applications of TiO$_2$, the main motivation in using rutile single-crystal samples in this study is its use as a prototypical surface science model system for transition metal oxides.[44] Although the gas-phase environment of the samples during our experiments is very different than most applied conditions, it enables detailed sample characterization not otherwise possible. These controlled conditions are needed to correlate experimental findings with computational methods. Such model systems uniquely allow a detailed atomistic understanding of complex surface phenomena and provide important test scenarios for verifying computational methods.

Both experimental observation and theoretical prediction indicate that adsorbed hydroxyl groups anchor Pd adatoms, therefore increasing the Pd diffusion barrier and decreasing cluster sintering. Consequently, on the hydroxylated surface, only small (1−3 atoms) Pd clusters form at low Pd concentrations, contrary to hydroxyl-free surfaces where larger 3D clusters form at similar Pd concentrations. DFT and ReaxFF results indicate that hydroxyl groups can be transferred from the oxide surface to Pd clusters as small as two atoms. The removal of hydrogen from the substrate enables Pd to freely diffuse and subsequently agglomerate into

larger clusters. MC simulations indicate that the H/Pd ratio in Pd clusters remains near ~0.65 for all cluster sizes. Hence, a significant number of hydroxyl groups remain on the surface at low Pd deposition times. As the Pd deposition time increases, fewer hydroxyls remain on the surface, which in turn allows small Pd clusters to readily diffuse and agglomerate. This leads to a bimodal cluster size distribution at intermediate deposition times, where enough hydroxyl groups have been adsorbed to allow significant Pd clusters to form, and the remaining hydroxyl groups hinder Pd diffusion, allowing small Pd clusters to persist on the surface.

As previous investigations have shown, hydroxyls may affect the sintering of metal clusters differently depending on the metal, the metal oxide support material, and potentially the crystallographic orientation of the surface. For example, studies of Au adsorbed on $TiO_2(110)$ suggest that adsorption of water on subsequent formation of hydroxyls facilitated sintering.[25] The situation on the $TiO_2(110)$ is, however, somewhat convoluted because adsorption of water in addition of forming hydroxyls also removes surface O vacancies, which are known to act as anchoring sites for metals.[45,46] Thus, the different sintering behavior may be a consequence of fewer O vacancies rather than hydroxyl formation. This problem is avoided in our experiments because the $TiO_2(011)$-2 × 1 is known to exhibit fewer O vacancies in vacuum-prepared surfaces[47] and hydroxyls are formed at the surface by adsorbing atomic hydrogen. Our results for Pd on $TiO_2(011)$-2 × 1 are similar to results for Pd on Fe_3O_4 that demonstrated suppressed Pd sintering on the hydroxylated surface. As our investigation shows, the mechanism of metal sintering has different contributions. An enhanced binding of adatoms to surface sites adjacent to hydroxyl groups and the associated increase in surface diffusion barriers are responsible for the initial suppression of Pd sintering. This metal–hydroxyl interaction will be different for different elements, and in some cases, a lower diffusion barrier may result. We speculate that this is possibly the case for Au on the hydroxylated $TiO_2(110)$ surface. The relatively weak adsorption of hydrogen on the $TiO_2(011)$-2 × 1 surface and the relatively strong Pd–H

bond in the metal hydride explain why hydrogen can be readily removed from the oxide surface by the Pd clusters. The removal of hydroxyls from the surface at high Pd coverage subsequently increases the Pd adatom mobility. Consequently, the same cluster size distribution as what was observed on the clean TiO_2-(011)-2 × 1 surface is obtained after the hydroxyl groups have been removed. Thus, hydroxyls affect the sintering only at low Pd coverages in the case studied here. Generally, the tendency of metal clusters to absorb hydrogen from the oxide surface negating any "anchoring" effect of small clusters by hydroxyls will depend on the tendency of the metal to form hydrides and on the hydrogen–oxide bond strength. For Pd on the hydroxylated $TiO_2(011)$-2 × 1 surface, both the weak hydrogen adsorption on the oxide[29] and the well-known tendency of Pd to form a hydride favor the transfer of hydrogen from the oxide to the Pd cluster. Other systems may not readily remove hydroxyl groups, and thus a cluster stabilization may be observed at higher metal coverages than those reported here. Therefore, a strategy to increase cluster stabilization may be to find oxide supports with strong hydroxyl bonds.

CONCLUSION

In conclusion, while the complex interactions observed here do not reveal a universal prediction for the role hydroxyls play either enhancing or inhibiting metal sintering, the limited data available suggest that, for Pd, a strong interaction with surface hydroxyls increases diffusion barriers, preventing sintering. In general, the agreement between the simulations and the experimental data shows that a good prediction of metal cluster sintering can be obtained by coupled DFT, kMC, and ReaxFF-MC simulations. This is promising for future efforts seeking to computationally screen metal–hydroxyl interactions in different oxide materials. Importantly, in the Pd/$TiO_2(011)$-2 × 1 system, hydroxylation of the surface enables the formation of room temperature stable single Pd adatoms, which without the hydroxyls would sinter into larger 3D clusters. Thus, hydroxylation is a viable approach for stabilizing single transition metals on oxide supports.

METHODS

Experimental Methods. The experiments were carried out in a UHV chamber with a base pressure in the low 10^{-10} Torr range. The chamber was equipped with facilities for substrate cleaning including an ion gun for ion sputtering of the sample with 1 keV Ar^+ ions and a radiative BN sample heater that allowed sample heating up to 800 °C. For sample characterization, the UHV chamber was equipped with low energy electron diffraction (LEED) and an Omicron variable temperature STM operated at room temperature. The TiO_2 samples used in this study were cleaned by repeated cycles of sputtering and annealing to 650 °C in vacuum. Sample cleanliness was checked by STM

prior to Pd deposition. Pd was evaporated from a home-built Pd source consisting of a Pd wire wrapped around a tungsten wire that could be heated by a direct current. We always deposited Pd with the sample cooled to room temperature. The deposition rate may be estimated from the STM images to ~6×10^{-3} atoms/(nm^2s), which can be expressed as one equivalent monolayer in ~30 min deposition time if we define one equivalent monolayer as 2 atoms per $TiO_2(011)$-1 × 1 unit cell.

The samples studied here are rutile $TiO_2(011)$ single crystals purchased from MTI corporation. Unlike the more frequently studied $TiO_2(110)$ surfaces, the $TiO_2(011)$ surface reconstructs into a 2 × 1 superstructure. Furthermore, vacuum-prepared

surfaces do not exhibit the high density of O vacancies like the (110) surface. Our previous studies showed that hydrogen adsorbs on the two-fold terminated oxygen atoms weakly to form terminating surface hydroxyls.[29] These hydroxyls appeared as bright protrusions in empty state STM images. In some samples, hydrogen was naturally present and no additional preparation was required to obtain a high hydrogen coverage. Alternatively, atomic hydrogen can be adsorbed at the surface. This has been achieved by utilizing a hot tungsten filament in 2×10^{-6} Torr H_2 background gas and the sample facing the filament. In this way, we obtained a maximum coverage of about 0.2 monolayers of hydrogen. Hydrogen can also be removed from the surface by exposure to 10^{-6} Torr O_2 at room temperature. Similar reaction of hydroxyls with O_2 has also been reported for the (110) surface.[48]

DFT Method. The Vienna ab initio simulation package (VASP) was implemented for all DFT calculations.[49,50] The projector-augmented wave (PAW) formalization was employed to treat atomic core regions[51] and valence configurations of $4d^{10}$ for Pd atoms, $2s^2 2p^4$ for O atoms, and $3p^6 3d^2 4s^2$ for Ti atoms. All calculations were spin-polarized. The Perdew–Wang (PW91) version of the generalized gradient approximation (GGA) was used to treat the exchange-correlation functional, and plane-wave basis sets were truncated at 450 eV. The TiO$_2$(011)-2 × 1 reconstructed surface was modeled in a 2 × 1 unit cell with three TiO$_2$ trilayers perpendicular to the surface, where the topmost trilayer consisted of the reconstructed surface and bottom trilayer was fixed during structural optimizations. A 15 Å vacuum layer was included, separating periodic images perpendicular to the surface. The convergence criterion for structural optimization was 0.05 eV Å^{-1} for atomic forces in all directions. The Monkhorst–Pack (MP) method[52] was employed to model the first Brillouin zone of all periodic calculations, where a 3 × 3 × 1 MP k-point spacing was employed. The gas-phase Pd atom reference for surface binding energies was modeled in a 45 Å × 45 Å × 45 Å periodic box, where solely the Γ point was considered. Transition states for Pd and H diffusion on the TiO$_2$ surface were identified by the climbing image nudged elastic band (CI-NEB) procedure implemented in VASP.[53]

We note that there is a well-known deficiency in the GGA-PW91 functional for describing localized Ti 3d states that may become partially occupied when the surface is reduced by adsorbed H atoms. This issue can be mitigated by the inclusion of the Hubbard U term, which prevents spurious delocalization of localized states.[54] To assess the impact of this deficiency, we conducted DFT+U calculations with a U value of 4.2 eV[55] applied to the 3d states of all Ti atoms. We found that the inclusion of U value yields similar Pd adsorption energies and higher Pd diffusion barriers. However, the relative trends in diffusion barriers remained the same as those identified when the U value was excluded. On the clean surface, the lowest diffusion barrier for Pd migration in the $[0\bar{1}1]$ direction was 31.9 kcal mol^{-1}, compared to the barrier of 35.0 kcal mol^{-1} on the hydroxylated surface. The difference of 3.1 kcal mol^{-1} yields a diffusion rate in the preferred direction parallel to the zigzag row ~1.9×10^2 times slower on the hydroxylated surface at 300 K, in qualitative agreement with the results obtained above without the U term. Tao *et al.*[29] similarly found that the inclusion of the Hubbard U term did not qualitatively affect H binding trends or relative diffusion barriers on this surface.

kMC Method. DFT energetics were used to derive Pd hopping rates during kMC simulations of Pd cluster formation on the TiO$_2$ surface. Diffusion rates were derived from harmonic transition state theory, where the activation barrier for each process was determined by cluster size and whether the move was within a trough or was over the zigzag row. For moves involving a Pd atom leaving a cluster, the barrier is increased by the sintering energy given by

$$E_{sinter} = E(Pd_{n-1} + Pd_1) - E(Pd_n) \qquad (1)$$

We applied sintering energies derived from the DFT data for cluster adsorption provided in Supporting Information Table S1, where the additional sintering energy was 19.2 kcal mol^{-1} to

TABLE 1. Rate Constants Determined from Harmonic Transition State Theory for Possible Move Types during kMC Simulations on the Clean and Hydroxylated TiO$_2$(011)-(2 × 1) Surface at 450 K

TiO$_2$-clean (move type)	cluster size (# atoms)	barrier (kcal mol^{-1})	sintering energy (kcal mol^{-1})	rate constant (s^{-1})
in trough	1 or 2	21.2		5.1×10^2
in trough	3	21.2	19.2	2.4×10^{-7}
in trough	≥4	21.2	15.6	1.3×10^{-5}
over row	1 or 2	24.0		2.2×10^1
over row	3	24.0	19.2	1.1×10^{-8}
over row	≥4	24.0	15.6	5.8×19^{-7}

TiO$_2$-(OH) move type	cluster size (# atoms)	barrier (kcal mol^{-1})	sintering energy (kcal mol^{-1})	rate constant (s^{-1})
in trough	1 or 2	24.1		1.9×10^1
in trough	3	24.1	19.2	9.3×10^{-9}
in trough	≥4	24.1	15.6	5.2×10^{-7}
over row	1 or 2	28.9		9.2×10^{-2}
over row	3	28.9	19.2	4.3×10^{-11}
over row	≥4	28.9	15.6	2.4×10^{-9}

remove a Pd atom from a Pd$_3$ cluster and was 15.6 kcal mol^{-1} to remove a Pd atom from a Pd$_4$ cluster. As seen in the table, there is little difference in adsorption energy per Pd atom between a single Pd monomer and a dimer, so no sintering energy was included in the barrier when a Pd atom is removed from a dimer. Furthermore, we assumed that the sintering energy was constant for Pd clusters larger than four atoms. This results in six processes with unique rates: (1) a move within the trough or (2) a move over the zigzag row; each coupled with (1) a move from a monomer or dimer, (2) a move from a Pd$_3$ cluster, or (3) a move from a Pd$_{n \geq 4}$ cluster. Finally, we conducted the simulations at a temperature of 450 K, which is high enough to induce sintering. We assume the usual pre-exponential factor of 10^{13} s^{-1}, which results in the rate constants provided in Table 1 for each of the six processes.

During each kMC step, a move is chosen from the following well-known kMC criteria derived from detail balance relationships:[56]

$$R = \sum_i n_i r_i \qquad (2)$$

$$\frac{1}{R} \sum_{i=0}^{k} n_i r_i \geq rand(0, 1) > \frac{1}{R} \sum_{i=0}^{k-1} n_i r_i \qquad (3)$$

where R is the sum of the rates of all possible processes, r_i is the rate of process i, and n_i is the number of available processes with rate r_i; r_k is the randomly selected rate, from which one of the processes with rate r_k is executed. The system time is then updated using the following:

$$t = t + \Delta t \quad \text{and} \quad \Delta t = -\frac{1}{R} \log[rand(0, 1)] \qquad (4)$$

where the time step of each move is inversely proportional to the overall rate total, R.

ReaxFF Potential and MC Method. The ReaxFF potential is a classical force-field method that is computationally inexpensive compared to *ab initio* total energy calculations, which enables studies on system models far larger than those typically employed for QM calculations.[57] The combination of both bonding and nonbonding interactions enables the potential to model van der Waals, Coulombic, and covalent interactions during reactive events, thus allowing simulations involving complex metal/oxide/gas interfaces.[58−62] This makes the ReaxFF potential ideal for modeling hydrogen uptake in large (~20 atom) Pd

clusters supported on an extensive (∼1000 atom) TiO_2 surface. The Ti/O/H,[63] Pd/O,[64] and Pd/H[42] interaction parameters employed here were developed previously. The Pd/O and Pd/H parameters have not been altered, whereas the O−H bond energy term was altered in the Ti/O/H description in order to properly reproduce H atom binding on the TiO_2-2 × 1 surface. The comparison between ReaxFF adsorption energies and the DFT training set reported previously by Tao et al.[29] is provided in Table S1 of the Supporting Information. The Ti/O/Pd three-body interaction terms were optimized against a training set consisting of Pd_n (n = 1−4) cluster adsorption energies on the $TiO_2(011)$-2 × 1 surface at varying sites, which is also provided in Table S2 of the Supporting Information. The complete Pd/Ti/O/H interaction potential and general parameters are provided in the Supporting Information in ReaxFF input format.

The optimized ReaxFF potential was employed in NVT-MC simulations in which the number of atoms (N), system volume (V), and system temperature (T) were fixed. Each MC step randomly displaced a H atom to a new location anywhere in the unit cell, and the resulting configuration was accepted or rejected according to the Metropolis probability criterion:[56,65] Prob = min[1,exp[−$\beta(E_2 − E_1)$]]. The system was considered converged if the total system energy did not change by more than 10 kcal mol^{-1} over the final 1000 MC trial iterations. As described previously,[64] a CG relaxation step prior to applying the Metropolis criterion is often necessary to increase the acceptance rates for "off-lattice" MC moves in which the displacement of one atom may require a structural relaxation in the surrounding system. This strategy was employed here to prevent wasted MC steps in which displaced H atoms are relocated to high energy positions within the atomic radius of the surrounding oxygen or metal atoms. The converged structure at the end of the simulation represents the equilibrated surface structure at the temperature set by the Metropolis criterion, which was 300 K for all MC simulations reported here.

REFERENCES AND NOTES

1. Qiao, B.; Wang, A.; Yang, X.; Allard, L. F.; Jiang, Z.; Cui, Y.; Liu, J.; Li, J.; Zhang, T. Single Atom Catalysis of CO Oxidation Using Pt_1/FeOx. *Nat. Chem.* **2011**, *3*, 634–641.

2. Lin, J.; Qiao, B.; Liu, J.; Huang, Y.; Wang, A.; Li, L.; Zhang, W.; Allard, L. F.; Wang, X.; Zhang, T. Design of a Highly Active Ir/Fe(OH)x Catalyst: Versatile Application of Pt-Group Metals for the Preferential Oxidation of Carbon Monoxide. *Angew. Chem., Int. Ed.* **2012**, *51*, 2920–2924.

3. Yang, X. F.; Wang, A.; Qiao, B.; Li, J.; Liu, J.; Zhang, T. Single-Atom Catalysts: A New Frontier in Heterogeneous Catalysis. *Acc. Chem. Res.* **2013**, *46*, 1740–1748.

4. Vajda, S.; Pellin, M. J.; Greeley, J. P.; Marshall, C. L.; Curtiss, L. A.; Ballentine, G. A.; Elam, J. W.; Catillon-Mucherie, S.; Redfern, P. S.; Mehmood, F.; *et al.* Subnanometre Platinum Clusters as Highly Active and Selective Catalysts for Oxidative Dehydrogenation of Propane. *Nat. Mater.* **2009**, *8*, 213–216.

5. Haruta, M. Size- and Support-Dependency in the Catalysis of Gold. *Catal. Today* **1997**, *36*, 153–166.

6. Valden, M.; Lai, X.; Goodman, D. W. Onset of Catalytic Activity of Gold Clusters on Titania with the Appearance of Nonmetallic Properties. *Science* **1998**, *281*, 1647–1650.

7. Lemire, C.; Meyer, R.; Shaikhutdinov, Sh. K.; Freund, H.-J. CO Adsorption on Oxide Supported Gold: From Small Clusters to Monolayer Islands and Three-Dimensional Nanoparticles. *Surf. Sci.* **2004**, *552*, 27–34.

8. Lee, S.; Fan, C.; Wu, T.; Anderson, S. L. CO Oxidation on Au_n/TiO_2 Catalysts Produced by Size-Selected Cluster Deposition. *J. Am. Chem. Soc.* **2004**, *126*, 5682–5683.

9. Sanchez, A.; Abbet, S.; Heiz, U.; Schneider, W. D.; Haekkinen, H.; Barnett, R. N.; Landman, U. When Gold Is Not Noble: Nanoscale Gold Catalysts. *J. Phys. Chem. A* **1999**, *103*, 9573–9578.

10. Landman, U.; Yoon, B.; Zhang, C.; Heiz, U.; Arenz, M. Factors in Gold Nanocatalysis: Oxidation of CO in the Non-scalable Size Regime. *Top. Catal.* **2007**, *44*, 145–158.

11. Herzing, A. A.; Kiely, C. J.; Carley, A. F.; Landon, P.; Hutchings, G. J. Identification of Active Gold Nanoclusters on Iron Oxide Supports for CO Oxidation. *Science* **2008**, *321*, 1331–1335.

12. Kaden, W. E.; Wu, T.; Kunkel, W. A.; Anderson, S. L. Electronic Structure Controls Reactivity of Size-Selected Pd Clusters Adsorbed on TiO_2 Surfaces. *Science* **2009**, *326*, 826–829.

13. Kaden, W. E.; Kunkel, W. A.; Kane, M. D.; Roberts, F. S.; Anderson, S. L. Size-Dependent Oxygen Activation Efficiency Over Pd_n/$TiO_2(110)$ for the CO Oxidation Reaction. *J. Am. Chem. Soc.* **2010**, *132*, 13097–13099.

14. Kaden, W. E.; Kunkel, W. A.; Roberts, F. S.; Kane, M.; Anderson, S. L. CO Adsorption and Desorption on Size Selected Pd_n/$TiO_2(110)$ Model Catalysts: Size Dependence of Binding Sites and Energies, and Support-Mediated Adsorption. *J. Chem. Phys.* **2012**, *136*, 204705.

15. Wörz, A. S.; Judai, K.; Abbet, S.; Heiz, U. Cluster Size-Dependent Mechanisms of CO+ NO Reaction on Small Pd_n (n < 30) Clusters on Oxide Surfaces. *J. Am. Chem. Soc.* **2003**, *125*, 7964–7970.

16. Fischer-Wolfarth, J. H.; Farmer, J. A.; Flores-Camacho, J. M.; Genest, A.; Yudanov, I. V.; Rösch, N.; Campbell, C. T.; Schauermann, S.; Freund, H.-J. Particle-Size Dependent Heats of Adsorption of CO on Supported Pd Nanoparticles as Measured with a Single-Crystal Microcalorimeter. *Phys. Rev. B* **2010**, *81*, 241416(R).

17. Kunz, S.; Schweinberger, F. F.; Habibpour, V.; Röttgen, M.; Harding, C.; Arenz, M.; Heiz, U. Temperature Dependent CO Oxidation Mechanisms on Size-Selected Clusters. *J. Phys. Chem. C* **2010**, *114*, 1651–1654.

18. Chambers, S. A.; Droubay, T.; Jennison, D. R.; Mattsson, T. R. Laminar Growth of Ultrathin Metal Films on Metal Oxides: Co on Hydroxylated α-$Al_2O_3(0001)$. *Science* **2002**, *297*, 827–831.

19. Kelber, J. A.; Niu, C.; Shepherd, K.; Jennison, D. R.; Bogicevic, A. Copper Wetting of α-$Al_2O_3(0001)$: Theory and Experiment. *Surf. Sci.* **2000**, *446*, 76–88.

20. Niu, C.; Shepherd, K.; Martini, D.; Tong, J.; Kelber, J. A.; Jennison, D. R.; Bogicevic, A. Cu Interactions with α-Al_2O_3-(0001): Effects of Surface Hydroxyl Groups *versus* Dehydroxylation by Ar-Ion Sputtering. *Surf. Sci.* **2000**, *465*, 163–176.

21. Bäumer, M.; Freund, H.-J. Metal Deposits on Well-Ordered Oxide Films. *Prog. Surf. Sci.* **1999**, *61*, 127–198.

22. Lai, X.; St. Clair, T. P.; Valden, M.; Goodman, D. W. Scanning Tunneling Microscopy Studies of Metal Clusters Supported on $TiO_2(110)$: Morphology and Electronic Structure. *Prog. Surf. Sci.* **1998**, *59*, 25–52.

23. Dulub, O.; Batzill, M.; Diebold, U. Growth of Copper on Single Crystalline ZnO: Surface Study of a Model Catalyst. *Top. Catal.* **2005**, *36*, 65–76.

24. Heemeier, M.; Frank, M.; Libuda, J.; Wolter, K.; Kuhlenbeck, H.; Bäumer, M.; Freund, H.-J. The influence of OH Groups on the Growth of Rhodium on Alumina: A Model Study. *Catal. Lett.* **2000**, *68*, 19–24.

25. Matthey, D.; Wang, J. G.; Wendt, S.; Matthiesen, J.; Schaub, R.; Laegsgaard, E.; Hammer, B.; Besenbacher, F. Enhanced Bonding of Gold Nanoparticles on Oxidized $TiO_2(110)$. *Science* **2007**, *315*, 1692–1696.

26. Parkinson, G. S.; Novotny, Z.; Argentero, G.; Schmid, M.; Pavelec, J.; Kosak, R.; Blaha, P.; Diebold, U. Carbon Monoxide-Induced Adatom Sintering in a Pd-Fe_3O_4 Model Catalyst. *Nat. Mater.* **2013**, *12*, 724–728.

27. Meyer, R.; Ge, Q.; Lockemeyer, J.; Yeates, R.; Lemanski, M.; Reinalda, D.; Neurock, M. An *Ab Initio* Analysis of Adsorption and Diffusion of Silver Atoms on Alumina Surfaces. *Surf. Sci.* **2007**, *601*, 134–145.

28. Meyer, R.; Lockemeyer, J.; Yeates, R.; Lemanski, M.; Reinalda, D.; Neurock, M. An *Ab Initio* Analysis of Adsorption and Diffusion of Silver Atoms on Partially Hydroxylated α-Al_2O_3-(0001) Surfaces. *Chem. Phys. Lett.* **2007**, *449*, 155–159.

29. Tao, J. G.; Cuan, Q.; Gong, X. Q.; Batzill, M. Diffusion and Reaction of Hydrogen on Rutile TiO_2(011)-2 × 1: The Role of Surface Structure. *J. Phys. Chem. C* **2012**, *116*, 20438–20446.

30. Beck, T. J.; Klust, A.; Batzill, M.; Diebold, U.; Di Valentin, C.; Selloni, A. Surface Structure of TiO_2(011)-(2 × 1). *Phys. Rev. Lett.* **2004**, *93*, 036104.

31. Torrelles, X.; Cabailh, G.; Lindsay, R.; Bikondoa, O.; Roy, J.; Zegenhagen, J.; Teobaldi, G.; Hofer, W. A.; Thornton, G. Geometric Structure of TiO_2(011)(2 × 1). *Phys. Rev. Lett.* **2008**, *101*, 185501.

32. Gong, X. Q.; Khorshidi, N.; Stierle, A.; Vonk, V.; Ellinger, C.; Dosch, H.; Cheng, H. Z.; Selloni, A.; He, Y. B.; Dulub, O.; *et al.* The 2 × 1 Reconstruction of the Rutile TiO_2(011) Surface: A Combined Density Functional Theory, X-ray Diffraction, and Scanning Tunneling Microscopy Study. *Surf. Sci.* **2009**, *603*, 138–144.

33. Cuan, Q.; Tao, J. G.; Gong, X. Q.; Batzill, M. Adsorbate Induced Restructuring of TiO_2(011)-(2 × 1) Leads to One-Dimensional Nanocluster Formation. *Phys. Rev. Lett.* **2012**, *108*, 106105.

34. Højrup Hansen, K.; Worren, T.; Stempel, S.; Lægsgaard, E.; Bäumer, M.; Freund, H.-J.; Besenbacher, F.; Stensgaard, I. Palladium Nanocrystals on Al_2O_3: Structure and Adhesion Energy. *Phys. Rev. Lett.* **1999**, *83*, 4120–4123.

35. Gong, X. Q.; Selloni, A.; Dulub, O.; Jacobsen, P.; Diebold, U. Small Au and Pt Clusters at the Anatase TiO_2(101) Surface: Behavior at Terraces, Steps, and Surface Oxygen Vacancies. *J. Am. Chem. Soc.* **2008**, *130*, 370–381.

36. Dulub, O.; Boatner, L. A.; Diebold, U. STM Study of Cu Growth on the ZnO(10−10) Surface. *Surf. Sci.* **2002**, *504*, 271–281.

37. Schmidt, A. A.; Eggers, H.; Herwig, K.; Anton, R. Comparative Investigation of the Nucleation and Growth of fcc-Metal Particles (Rh, Ir, Ni, Pd, Pt, Cu, Ag, Au) on Amorphous Carbon and SiO_2 Substrates during Vapor Deposition at Elevated Temperatures. *Surf. Sci.* **1996**, *349*, 301–316.

38. Zhang, J.; Alexandrova, A. N. Structure, Stability, and Mobility of Small Pd Clusters on the Stoichiometric and Defective TiO_2(110) Surfaces. *J. Chem. Phys.* **2011**, *135*, 174702.

39. Ingham, B.; Toney, M. F.; Hendy, S. C.; Cox, T.; Fong, D. D.; Eastman, J. A.; Fuoss, P. H.; Stevens, K. J.; Lassesson, A.; Brown, S. A.; *et al.* Particle Size Effect of Hydrogen-Induced Lattice Expansion of Palladium Nanoclusters. *Phys. Rev. B* **2008**, *78*, 245408.

40. Eastman, J. A.; Thompson, L. J.; Kestel, B. J. Narrowing of the Palladium−Hydrogen Miscibility Gap in Nanocrystalline Palladium. *Phys. Rev. B* **1993**, *48*, 84–92.

41. Jewell, L. L.; Davis, B. H. Review of Absorption and Adsorption in the Hydrogen−Palladium System. *Appl. Catal., A* **2006**, *310*, 1–15.

42. Senftle, T. P.; Janik, M. J.; van Duin, A. C. T. A ReaxFF Investigation of Hydride Formation in Palladium Nanoclusters *via* Monte Carlo and Molecular Dynamics Simulations. *J. Phys. Chem. C* **2014**, *118*, 4967–4981.

43. Luttrell, T.; Halpegamage, S.; Tao, J. G.; Kramer, A.; Sutter, E.; Batzill, M. Why Is Anatase a Better Photocatalyst than Rutile? Model Studies on Epitaxial TiO_2 Films. *Sci. Rep.* **2014**, *4*, 4043.

44. Diebold, U. The Surface Science of Titanium Dioxide. *Surf. Sci. Rep.* **2003**, *48*, 53–229.

45. Lee, S.; Fan, C.; Wu, T.; Anderson, S. L. Agglomeration, Support Effects, and CO Adsorption on Au/TiO_2 (110) Prepared by Ion Beam Deposition. *Surf. Sci.* **2005**, *578*, 5–19.

46. Wendt, S.; Schaub, R.; Matthiesen, J.; Vestergaard, E. K.; Wahlström, E.; Rasmussen, M. D.; Thostrup, P.; Molina, L. M.; Lægsgaard, E.; Stensgaard, I.; *et al.* Oxygen Vacancies on TiO_2(1 1 0) and Their Interaction with H_2O and O_2: A Combined High-Resolution STM and DFT Study. *Surf. Sci.* **2005**, *598*, 226–245.

47. Dulub, O.; Di Valentin, C.; Selloni, A.; Diebold, U. Structure, Defects, and Impurities at the Rutile TiO_2(011)-(2 × 1) Surface: A Scanning Tunneling Microscopy Study. *Surf. Sci.* **2006**, *600*, 4407–4417.

48. Papageorgiou, A. C.; Beglitis, N. S.; Pang, C. L.; Teobaldi, G.; Cabailh, G.; Chen, Q.; Fisher, A. J.; Hofer, W.; Thornton, G. Electron Traps and Their Effect on the Surface Chemistry of TiO_2(110). *Proc. Natl. Acad. Sci. U.S.A.* **2010**, *107*, 2391.

49. Kresse, G.; Furthmüller, J. Efficiency of *Ab-Initio* Total Energy Calculations for Metals and Semiconductors Using a Plane-Wave Basis Set. *Comput. Mater. Sci.* **1996**, *6*, 15–50.

50. Kresse, G.; Furthmüller, J. Efficient Iterative Schemes for *Ab Initio* Total-Energy Calculations Using a Plane-Wave Basis Set. *Phys. Rev. B* **1996**, *54*, 11169–11186.

51. Kresse, G.; Joubert, D. From Ultrasoft Pseudopotentials to the Projector Augmented-Wave Method. *Phys. Rev. B* **1999**, *59*, 1758–1775.

52. Monkhorst, H. J.; Pack, J. D. Special Points for Brillouin-Zone Integrations. *Phys. Rev. B* **1976**, *13*, 5188–5192.

53. Henkelman, G.; Uberuaga, B. P.; Jonsson, H. A Climbing Image Nudged Elastic Band Method for Finding Saddle Points and Minimum Energy Paths. *J. Chem. Phys.* **2000**, *113*, 9901–9904.

54. Dudarev, S. L.; Botton, G. A.; Savrasov, S. Y.; Humphreys, C. J.; Sutton, A. P. Electron-Energy-Loss Spectra and the Structural Stability of Nickel Oxide: An LSDA+U Study. *Phys. Rev. B* **1998**, *57*, 1505–1509.

55. Cococcioni, M.; de Gironcoli, S. Linear Response Approach to the Calculation of the Effective Interaction Parameters in the LDA+U Method. *Phys. Rev. B* **2005**, *71*, 035105.

56. Frenkel, D.; Smit, B. *Understanding Molecular Simulation: From Algorithms to Applications*; Academic Press: San Diego, CA, 2002.

57. van Duin, A. C. T.; Dasgupta, S.; Lorant, F.; Goddard, W. A., III. ReaxFF: A Reactive Force Field for Hydrocarbons. *J. Phys. Chem. A* **2001**, *105*, 9396–9409.

58. Lahiri, J.; Mayernick, A. D.; Morrow, S. L.; Koel, B. E.; van Duin, A. C. T.; Janik, M. J.; Batzill, M. Modification of Active Sites on YSZ(111) by Yttria Segregation. *J. Phys. Chem. C* **2009**, *114*, 5990–5996.

59. Chenoweth, K.; van Duin, A. C. T.; Persson, P.; Cheng, M.-J.; Oxgaard, J.; Goddard, W. A., III. Development and Application of a ReaxFF Reactive Force Field for Oxidative Dehydrogenation on Vanadium Oxide Catalysts. *J. Phys. Chem. C* **2008**, *112*, 14645–14654.

60. Chenoweth, K.; van Duin, A. C. T.; Goddard, W. A., III. The ReaxFF Monte Carlo Reactive Dynamics Method for Predicting Atomistic Structures of Disordered Ceramics: Application to the Mo_3VO_x Catalyst. *Angew. Chem., Int. Ed.* **2009**, *48*, 7630–7634.

61. Monti, S.; van Duin, A. C. T.; Kim, S.-Y.; Barone, V. Exploration of the Conformational and Reactive Dynamics of Glycine and Diglycine on TiO_2: Computational Investigations in the Gas Phase and in Solution. *J. Phys. Chem. C* **2012**, *116*, 5141–5150.

62. Raymand, D.; van Duin, A. C. T.; Spångberg, D.; Goddard, W. A., III; Hermansson, K. Water Adsorption on Stepped ZnO Surfaces from MD Simulation. *Surf. Sci.* **2010**, *604*, 741–752.

63. Raju, M.; Kim, S.-Y.; van Duin, A. C. T.; Fichthorn, K. A. ReaxFF Reactive Force Field Study of the Dissociation of Water on Titania Surfaces. *J. Phys. Chem. C* **2013**, *117*, 10558–10572.

64. Senftle, T. P.; Meyer, R. J.; Janik, M. J.; van Duin, A. C. T. Development of a ReaxFF Potential for Pd/O and Application to Palladium Oxide Formation. *J. Chem. Phys.* **2013**, *139*, 044109–044115.

65. Metropolis, N.; Rosenbluth, A. W.; Rosenbluth, M. N.; Teller, A. H.; Teller, E. Equation of State Calculations by Fast Computing Machines. *J. Chem. Phys.* **1953**, *21*, 1087–1092.